2024 IEEE International Conference on Robotics and Automation (ICRA 2024)
May 13-17, 2024. Yokohama, Japan

A non-magnetic dual-mode linear pneumatic actuator: initial design and assessment

Timothée Portha[1*], Laurent Barbé[1], François Geiskopf[1], Jonathan Vappou[1] and Pierre Renaud[1]

***Abstract*— A pneumatic linear actuator is presented and evaluated. Designed to operate in demanding environments such as MRI, it is developed to be used with two motion control modes: 1) a step-by-step mode with tooth-based gripping to ensure precision, 2) a continuous mode available locally for fine positioning. The actuator can also be disengaged to enable direct handling by an operator, for example for comanipulation. The design is presented. A prototype, developed in the medical context, is implemented and characterized. A specific step-by-step control sequence is then elaborated based on its characterization. Testing of the dual-mode actuation is finally described. The complementarity between the two motion modes and possible adaptations of the original design are discussed.**

I. Introduction

The added value of robotic systems in the medical field was proven for various applications. Image-guided robotics are of particular interest when precision and accuracy are needed for tasks such as position control of needles [1], [2] or HIFU (High Intensity Focused Ultrasound) probes [3], [4], [5]. The MRI environment is particularly challenging for the design of robotic systems: depending on the material susceptibility, robot body can cause artefacts in the image, and many sensors and actuators can disturb the image as well [6]. Furthermore, the available space in the tunnel is limited. Many designs of actuators have thus been introduced using piezoelectric actuators [7], [8]. Another relevant approach is fluidic actuation coupled with a polymer-based design [9], [10], which can ensure MR-compatibility [11]. This association is of interest in a broader field of applications, as it is also suitable for instance in explosive environment [12].

Several designs of rotary actuators have been proposed [13], [14], [15], [16] with step-by-step kinematics. Such kinematics are of interest for the possible unlimited range of motion. Linear motion can then be produced if the actuator is connected to a transformation mechanism [17]. This, however, can degrade the compactness and mechanical efficiency. A few fluidic linear actuator designs have been proposed. In [18], [19], [5] rolling diaphragms are used. The absence of friction is of great interest, but the range of motion remains limited, as it is with cylinder-based actuation [20]. Linear step-by-step pneumatic actuation seems particularly relevant. It is achieved in [10], with an actuation solution for needle insertion. Inchworm kinematics, a step-by-step strategy, are adopted with gripping of the needle by friction. The actuator offers the possibility to decouple the moving element from the actuator for complete removal. This is an important safety feature which also allows direct handling by the user. The forward motion is provided by the pressurization of a central chamber. However, the step-by-step motion sequence provides a motion that is not continuous. A continuous motion could be feasible if the central pneumatic chamber provides a sufficient range of motion. Fine positioning would then be possible, in conjunction with unlimited range of motion provided by inchworm kinematics. To the best of our knowledge, such a combination has not been exploited yet. Also, the design is based on friction-based grippers to grasp the moving element which has some limitations, and most notably the possible appearance of sliding, causing a loss of accuracy.

The actuator presented in [21] also uses step-by-step motion. This solution is of great interest for its position accuracy: the motion is generated using obstacles, via the use of gear racks, i.e. toothed elements, that come into contact to generate force and then motion. This solves the problem related to the use of friction-based grippers. However, the design of the toothed elements can be delicate. The actuator resolution is linked to the pitch of the gears. The generated force is directly dependent on the relative motion between the racks, so friction has to be managed. Moreover, a permanent contact between the tooth of the fixed and moving parts is maintained, rendering disengagement impossible.

In this article, we assess the interest of a hybrid actuation approach to design a linear pneumatic actuator, combining the relevant characteristics of the two previous solutions. The proposition is to have a dual-mode linear actuation: 1) a step-by-step motion with tooth-based force transmission for accuracy and unlimited range of motion and 2) a continuous motion on a specific range of motion for fine positioning, using a central pneumatic chamber. The actuator behavior is evaluated based on a prototype, developed for HIFU probe position control. In section II, the design and implementation are presented. The prototype characterization is then presented in section III and a specific step-by-step motion sequence is established. The motion modes are evaluated in section IV, before discussing in section V the interest of the solution and its possible adaptation in other contexts.

II. Design and implementation of the actuator

A. Principle of the two actuation modes

The structure of the actuator is presented in Fig. 1. This linear actuator is composed of three active elements: two grippers, and one central chamber. The grippers are mounted

*Corresponding author: timothee.portha@etu.unistra.fr
[1]ICube, University of Strasbourg, CNRS, INSA Strasbourg, France
This work was supported by ANR (Labcom TechnoFUSLab ANR-21-LCV3-0007-01), INSA Strasbourg and the Investissements d'Avenir program (TIRREX ANR-21-ESRE-0015, Labex CAMI ANR-11-LABX-0004).

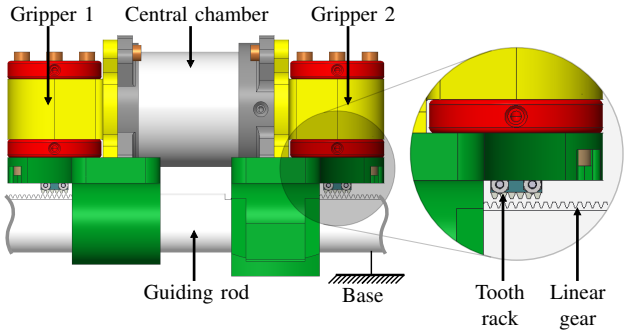

Fig. 1. CAD view of the actuator

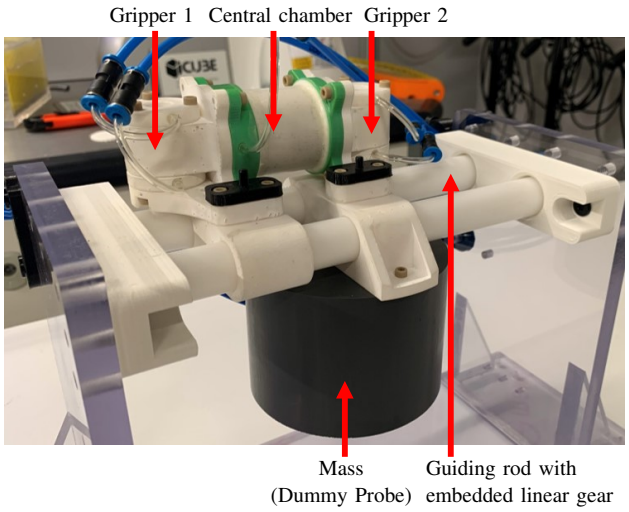

Fig. 2. Prototype of the actuator during characterization

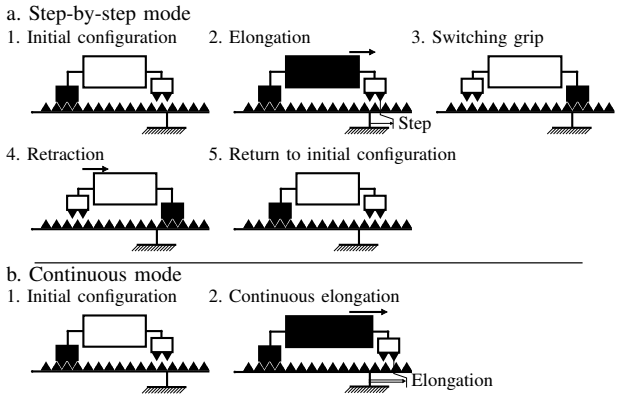

Fig. 3. Schematic representation of the 2 modes of motion. Activated components are in black.

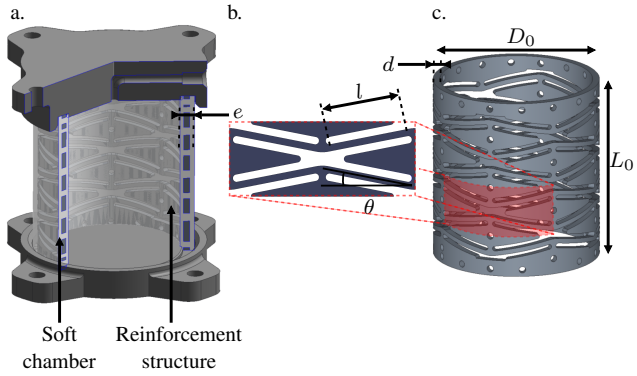

Fig. 4. a. CAD view of the central chamber, partial section. b. Unit cell of the structure. c. CAD view of the internal structure.

on a guiding rod, so they can translate with respect to the base. They are equipped with tooth racks at their tips. When activated pneumatically, the gripper ends are placed in contact with a rack installed on the guiding rod, to secure their position along the axis. The central chamber is also activated pneumatically. Its inflation causes an elongation in the direction of the guiding rod. By controlling independently the activation of the 2 grippers and the central chamber, two modes of actuation are developed.

A first mode, designated as the "step-by-step mode", is available by exploiting inchworm kinematics. The motion sequence can be depicted in Fig. 3.a. Starting from a position with one gripper closed and the other opened (State 1.), the central chamber elongates under pressure to shift the moving gripper of one step, which is equal to the tooth pitch of the gear rack (State 2.). The opened gripper closes and the closed one opens (State 3.), to let the central chamber retract (State 4.). The grippers switch again back to the initial configuration (State 5.). The next iteration of the sequence can then begin. The gear rack is used to impose a step-by-step motion, whose steps are accurately controlled, in comparison with friction-based grippers [10]. Thanks to the independent control of the active elements, it is also possible to disengage the two grippers simultaneously. The actuator can then be freely moved along the axis by a user, if co-manipulation is desired for instance.

In a second mode, designated in the following as the "continuous mode", depicted in Fig. 3.b, one gripper is initially activated before using the central chamber to obtain a translation. The central chamber is used to adjust the position of the moving gripper. The stroke is limited by the central chamber capability, but on the other hand, it is possible to generate a continuous motion, with a resolution that is not linked to the gear rack parameters, for a fine positioning.

The interest of the dual-mode actuator for motion control is investigated with an experimental approach. A prototype is thus built. It is designed in the context of MRI-guided HIFU, for probe motion control. The main specifications are issued from that context, namely: the displacement inside a MRI bore of a 0.8 kg probe, with velocity in the order of 1 mm/s, i.e. in quasi-static conditions. Due to MRI environment, 10 m long tubes are needed for transmitting pressured air to the actuator from the control room. Resolution in step-by-step motion needs to be around 2 mm. The prototype, represented in Fig. 2, comprises the actuator, the probe and a second guiding rod, to improve the translation accuracy of the probe. This prototype is comprised in a volume of 106 mm large, 129 mm long and 79 mm high with 45 mm above the guiding rod, for a weight of 420 g. The main design choices for the active components are described in the following paragraphs.

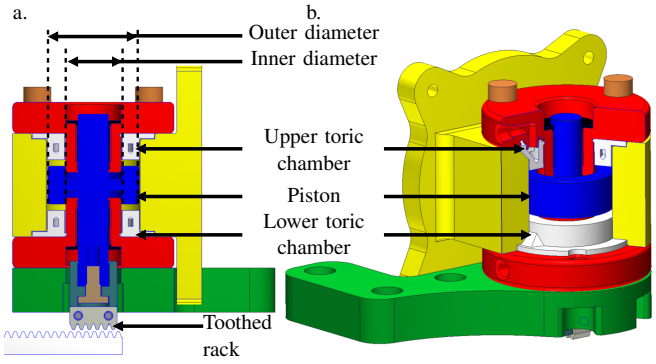

Fig. 5. a. CAD Section of a gripper. b. 3D view of a gripper, partial section

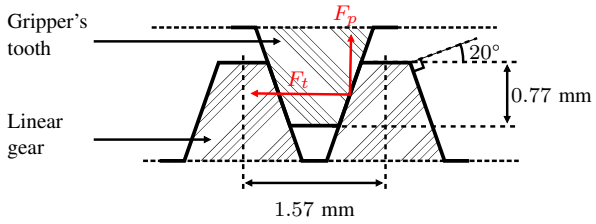

Fig. 6. Linear gear design

B. Central chamber

The central chamber is designed as a soft inflatable chamber with a reinforcement truss structure to favor the axial elongation (Fig. 4.a.). The springback effect of the soft chamber and the reinforcement structure is used for the central chamber retraction. The reinforcement structure (Fig. 4.c) is based on an inverted honeycomb shape pattern, as introduced in [10]. With this pattern, the motion is obtained by the bending of the oblique beams of length l (Fig. 4.b), initially at an angle θ. There are respectively N_c and N_v repetitions of the pattern along the circumference and the axial direction. The chamber nominal diameter and length are noted D_0 and L_0. The thickness of the structure and the overall wall thickness are designated by parameters d and e.

For the prototype, the diameter and length are chosen equal to 35 mm to keep the actuator compact, so it can be used inside the MRI bore. The selection of the parameters is the result of the analysis achieved in [22]. The truss structure parameters are selected to obtain an elongation close to twice the desired resolution, i.e. 4 mm. Selected values are equal to $(N_c,\, N_v,\, \theta,\, d) = (4,\, 3,\, 11°,\, 1.5\text{ mm})$. With these values, using PVC for the reinforcement structure and silicone for the soft chamber, whose Young's moduli are equal to 4.14 GPa and 0.7 MPa respectively, the predicted elongation is 4.4 mm for a pressure of 0.6 bar.

The reinforcement structure is CNC machined using PVC material. It is encompassed in a silicone rubber (RTV 3428) envelope, using overmolding technique.

C. Grippers

The grippers clench on a standard rack, in order to transmit the force developed by the central chamber. The gripper force capability depends on the solution for its pneumatic activation, and the geometry of the teeth. A 2-way activation of the grippers is selected to favor their dynamics. The design is represented in Fig. 5. Two toric pneumatic chambers are placed around the piston of each gripper. This solution reduces the friction encountered with a gasket-based solution. Moreover, the implementation of deformable chambers can be performed using 3D printing with a soft material, here silicone. The two chambers and the piston are encased in an outer envelope guiding the piston and constraining the inflation of the toric chamber in the direction of the piston displacement. The inflation of each of the chambers either elevates or lowers the piston while developing the necessary clenching force.

The rack is of normalized geometry. The pressure angle α has a standard value of 20°. The pitch of the rack is chosen equal to 1.57 mm among standard available values, to respect the condition on the resolution in the first mode of actuation. The displacement of the grippers must then exceed 0.77 mm as shown in Fig. 6. The design allows an excursion of 1 mm. The gripper is designed to have its outer dimensions close to the dimensions of the central chamber sides, to ease the integration. This leads to outer and inner diameters of the piston respectively equal to 17.1 mm and 12.5 mm. The pressure applied in the toric chambers is chosen to grip the rack while sustaining the force F_t developed by the central chamber. With $D_i = D_0 - e$ the inner diameter of the central chamber, this force F_t is equal to

$$F_t = \pi \frac{D_i^2}{4} P_{cc} \tag{1}$$

with P_{cc} the pressure. With $e = 3.5$ mm and input pressure of 0.6 bar as defined above, $F_t = 48$ N. Following Fig. 6, and neglecting friction between the piston and rack teeth, the force F_p exerted on the piston by the rack is equal to $F_p = F_t \tan\alpha$. This leads to a required force $F_p = 18$ N. The contact surface between the piston and each toric chamber is equal to 107 mm^2. Using a safety factor of 2, the pressure in the toric chambers is chosen equal to 3.5 bar.

Except the toothed components, the gripper structure is 3D printed, using Polyjet process (VeroWhite, Stratasys) for the piston, SLA process (Resin 10k, Formlabs) for the casing.

III. Control Strategy

A. Exploitation of the central chamber expansion

The central chamber is designed to be used in the continuous mode with an elongation larger than the step size defined by the rack pitch. In the step-by-step mode, using a pressure level to generate a steady-state elongation of one step could be sufficient to implement the sequence depicted in Fig. 3. However, the dynamics of the chamber available at higher pressure levels would then not be used. Our approach is then to use the chamber with a pressure level that should cause an elongation larger than the rack pitch, and work to adjust the instant when the moving gripper is closed, so grasping occurs

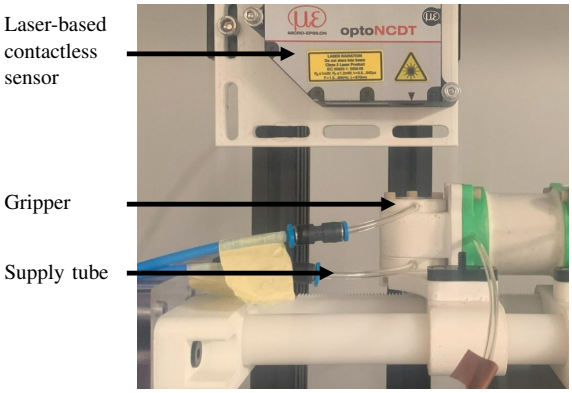

Fig. 7. Experimental setup for the characterization of grippers

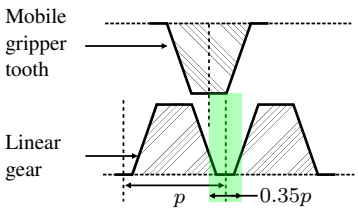

Fig. 8. Representation in green of the region where the gearing between the gripper and the rack is correct. p designates the pitch of the gear rack

TABLE I

CENTRAL CHAMBER ELONGATION AS A FUNCTION OF THE PRESSURE

Pressure (bar)		0.2	0.4	0.6	0.8	1.0	1.2
Elongation (mm)	Mean	0.98	1.84	2.90	3.94	4.91	5.78
	Std	0.08	0.11	0.15	0.19	0.13	0.10

after one step of elongation. In other words, with this dual-mode actuator, the gripper will be closed while the chamber still elongates, to better use the central chamber dynamics.

The control strategy requires a time synchronization between the different pneumatic chambers of grippers and central chamber, which have distinct dynamics. The latter need then to be characterized.

B. Characterization of components

1) Prototype instrumentation: All measurements were carried out on a pneumatic bench equipped with servo-valves (VPPM-6L, Festo AG), in order to ensure controlled pressure, and high-speed solenoid valves (MHE2-MS1H-3/2G, Festo AG) coupled to each pneumatic chamber to activate pressurization. The whole system is controlled by an on-board PC using a Xenomai real-time operating system with an acquisition task clocked at a frequency of 500 Hz. The pneumatic chambers are connected to the bench using tubes of 10 m length (4 mm x 0.75 mm, Festo AG). We equipped the pneumatic bench with a laser-based contactless sensor (OptoNCDT 2300-20, MicroEpsilon, 0.3 µm) to characterize the displacement and time responses.

2) Characterization of grippers: Two response times define the grippers behavior: the opening time t_o, needed by the piston to reach a displacement of 0.77 mm necessary to free the rack, and the closing time t_c, to move down the piston below 0.77 mm, to grasp the rack.

The two grippers are evaluated individually using the experimental bench shown in Fig. 7, where the laser sensor enables a direct measurement of the gripper's piston displacement. Tests were carried out with a supply pressure of 3.5 bar in each chamber. Each piston effectively reaches a displacement of at least 0.77 mm. The measured values for t_o and t_c are summarized in Tab. II with mean value, standard deviation, min and max values. Some slight differences between the two grippers can be noticed, probably due to the manufacturing process. The standard deviation does not exceed 1.4%(1.6%) of the mean opening (closing) times. Considering the range of opening and closing times, one can see that selecting $t_o = 370$ ms and $t_c = 220$ ms allows us to ensure correct actions for both grippers. These values are thus considered when designing the actuation sequence.

3) Characterization of the central chamber: Two actuation times are assessed for the central chamber: the elongation time t_e and the retraction time t_r. To define them, the gripping phase using the gear rack needs to be considered. With a standard gear geometry, the gearing remains correct only if the gripper teeth are positioned within a region whose width is 35% of the gear pitch, around the elongation of a step (Fig. 8). Adding some safety margins, it is considered that the centerline of the mobile tooth has to remain in a tolerance region which width is 30% of the gear pitch. Two values are thus estimated for the elongation time: the value to get a displacement of 85% of the pitch value, and the one to get 115%. If chosen between those boundaries, the elongation time will ensure a correct gearing. The analysis is similar for retraction. However, one boundary of the chamber displacement is set by the design, so only one retraction time t_r is measured.

Fig. 9 shows the experimental setup used to characterize the elongation chamber. The laser-based contactless sensor is positioned horizontally, pointing at one side of the elongation chamber. The elongation of the chamber was first verified under different pressures. The resulting elongations are presented in Tab. I, in terms of mean value and standard deviation. With a pressure of 0.6 bar, the elongation is already close to twice the step value, defined by the rack pitch. Following the principle introduced in III.A., this pressure is used from now on to ensure that the gripper closes while the chamber still elongates, to take advantage of the chamber dynamics.

We then evaluate the elongation and retraction response times. The values are reported in Tab. II. It should be noted that $t_e = 450$ ms and $t_r = 600$ ms respect the identified boundaries, to ensure the correct elongation and retraction of the central chamber. These values are thus considered to design the actuation sequence.

C. Actuation sequence

The characterization of the actuator components makes it possible to construct an actuation sequence for the actuation mode 1. The timeline in Fig. 10 shows the states that make up

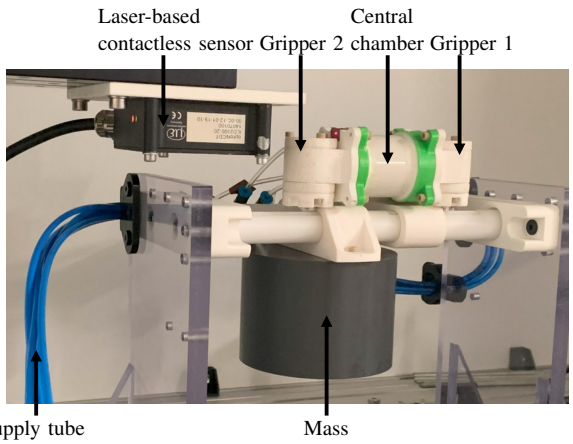

Fig. 9. Experimental setup during the characterization of the central chamber

TABLE II

MEASUREMENTS OF ACTUATION TIMES

	Chamber			Gripper 1		Gripper 2	
Actuation times (ms)	$t_{e,85\%}$	$t_{e,115\%}$	t_r	t_o	t_c	t_o	t_c
Mean	322	580	584	352	179	358	217
Std	11	65	5	5	3	3	1
Min	310	518	578	348	172	350	216
Max	342	718	594	364	182	362	218

the sequence. It is an adaptation of the inchworm sequence proposed in Fig. 3.a, in particular to synchronize the states. The approach here is not to exploit any feedback on the position of the central chamber. It is therefore imperative to actuate the gripper 2 for it to be closed at the instant the central chamber's elongation equals the length of one step at the end of state (E_1). However, this must be done taking into account the time required for the gripper piston to close (t_c) on the gear rack. Similarly, when activating the central chamber (state E_0), it must be ensured that gripper 1 is closed and gripper 2 is open, taking into account the activation time required for the latter to open (t_o) during state (E_6). Finally, when the central chamber retracts, the time to close the gripper 1 must be taken into account for it to be closed at the moment the central chamber has retracted at the end of state (E_4). For this sequence to be implemented, all the states have to be defined and of positive duration, i.e. the following conditions, as in our context, have to be verified : $t_e - t_c > 0$ and $t_r - t_c > 0$.

In order to control the actuator velocity, a state (E_2) of duration t_w has been introduced. The different response times for the central chamber (t_e and t_r) and grippers (t_o and t_c) are fixed parameters, as are the pressures (0.6 bar for the central chamber and 3.5 bar for the grippers). The waiting time t_w then allows us to modify the overall sequence period with

$$T = t_e + t_r + 2t_o + t_w \tag{2}$$

During this duration T, the actuator advances by one step p, so the average speed is $V = p/T$. The maximum speed is obtained with $t_w = 0$ ms. With the current prototype

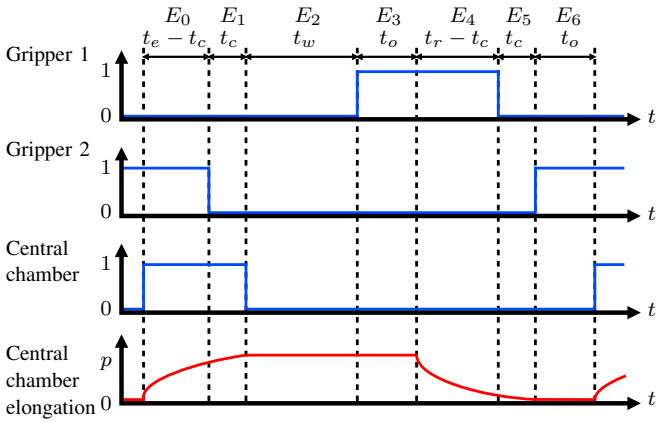

Fig. 10. Chronogram of the actuation sequence. In blue, the control signals of each pneumatic element (Grippers, 0::close, 1::open, Central chamber 0::unpressurized, 1::pressurized). In red, the elongation on the central chamber

and chosen actuation times, the maximum speed is thus 0.88 mm/s, which is within the required order of magnitude for the application under consideration.

IV. DUAL-MODE ASSESSMENT

A. Mode 1: Step-by-step motion

The actuator has been assessed in this mode using two different average speed values, 0.4 and 0.8 mm/s. This represents a duration of the motion sequences of respectively 3.9 and 2.0 seconds. The actuator displacement is analyzed using the same setup as for central chamber characterization. Results are represented in Fig. 11. The reference profiles of the position are in plotted lines, the measured positions in plain lines. Each motion sequence starts after a new step in the reference profile. To assess the accuracy of displacement, we focus on the time period corresponding to the state 5 in Fig. 10, which is the situation where both grippers are closed and the central chamber is at rest. The errors are equal to -0.007 ± 0.086 mm at 0.4 mm/s and -0.006 ± 0.059 mm at 0.8 mm/s. Before state 5, one can notice some errors, that can also be visualized on the attached video. They seem to be due to some kinematic errors due to the backlash between the gripper and guiding bars, creating some parasitic rotational motion.

Stopping the sequence in state 5 or 6 makes it possible to open simultaneously the two grippers. It is then possible to modify the position of the actuator manually , as illustrated in the attached video.

B. Mode 2: Continuous motion

The capacity to generate displacements of various amplitudes by modifying the pressure level was verified by activating the gripper 1, and activating the central chamber. With the setup described earlier, the actuator displacement was recorded to assess the feasible displacement for trapezoidal pressures profiles between 0 bar and 1.2 bar. The resulting elongation is shown in Fig. 12 for two temporal evolutions with different durations, as reported in the figure.

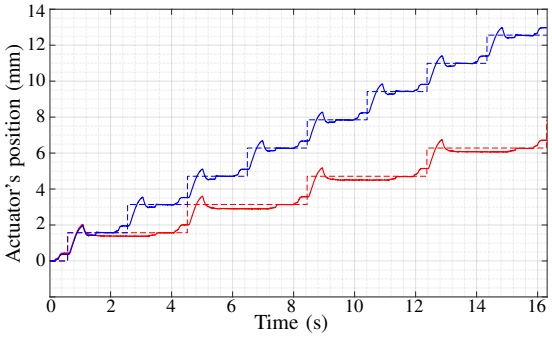

Fig. 11. Comparison of piece-wise step references and measured actuator displacements: in red for an average speed value of 0.4 mm/s, in blue for 0.8 mm/s.

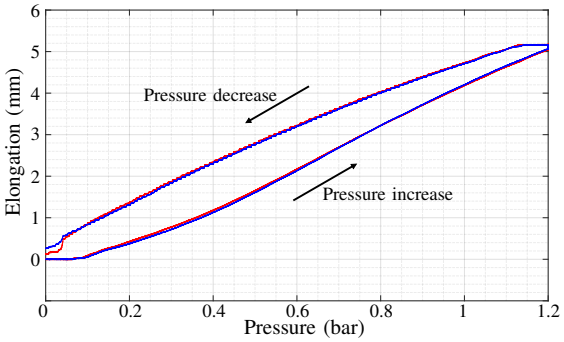

Fig. 12. Elongation obtained for two trapezoidal pressure profiles applied in the central chamber. Red curve: pressure increase to 120 s, constant for 30 s, pressure decrease in 120 s. Blue curve: pressure increase to 30 s, constant for 5 s, pressure decrease in 30 s

The actuator displacement remains repeatable between the two cycles. During the pressure increase, the elongation varies almost linearly from 0.2 bar to 1.2 bar. The non-linearity below 0.2 bar is related to the servo-valve dynamics, its range of pressure regulation ranging from 0.1 bar to 10 bar. Hysteresis is observed, probably due to the non-linear behavior of reinforced structure and friction in the guiding rods. We can indeed observe some stick-slip effect during pressure decrease. The actuator can provide a displacement up to 5.2 mm, which represents 3.3 steps achieved in mode 1.

The elongation capability can be used after a step-by-step motion. It could also be used for sequential motion, by achieving a "multi-step" motion. This is tested in Fig. 13 where a pressure of 0.8 bar is applied to generate an elongation equal to two times the rack pitch. It is compared to a reference piecewise-constant profile with $1.57 \times 2 = 3.14$ mm steps. The positioning error is -0.014 ± 0.020 mm at 0.92 mm/s. The continuous motion mode makes it also possible to obtain a step-by-step displacement on adjustable step lengths.

V. Conclusion

In this article, we have proposed an actuator architecture to perform a dual-mode linear motion, using either step-by-step kinematics, or a continuous motion over a reduced stroke. A prototype was designed to meet needs related to a medical context. This device was characterized to implement

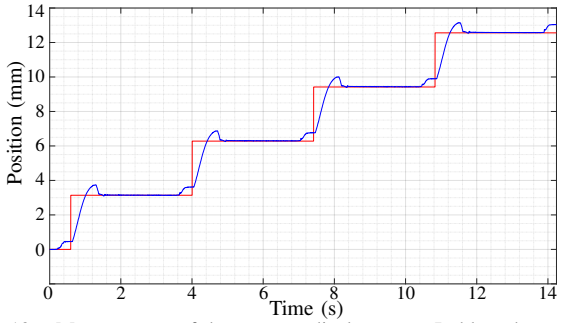

Fig. 13. Measurement of the actuator displacement. In blue, the measured displacement of the central chamber and in red the reference position.

a specific step-by-step sequence, and was then tested. The specific and complementary characteristics of the 2 operating modes were confirmed by experimental results. Thanks to the gearing, the stepper mode offers accuracy, with step errors less than 0.9% of the rack's pitch. For the proposed design, the continuous mode allows an effective displacement of 5.2 mm under 1.2 bar, which is significant and helpful to adjust the position. We also found that the central chamber could be operated in a "multi-step" mode, advancing from several steps during one motion sequence.

From an applicative point of view, the constraints related to the positioning of a HIFU transducer are satisfied: the motion of the probe is obtained with the desired speed and resolution, despite the presence of substantial pneumatic transmission lengths. For other contexts, the actuator characteristics are adjustable. If the speed requirement is higher, the volumes of the pneumatic chambers should be minimized. For the central chamber, this can be achieved by reducing the diameter for the same length. Conversely, the diameter of the chamber and pistons is the main factor for force generation. Through diameter modification, it should then be possible to adjust the force/speed balance. At the same time, the pitch of the rack determines the resolution achievable with the actuator in stepper mode, so it is straightforward to adjust. One perspective is to formalize a design method for such actuator adaptation.

Other perspectives of the work concern the control of the actuator. The elongation of the central chamber for a given pressure is repeatable. However, the retraction, due to the springback effect of the reinforced structure, is subject to non-linearities. It would be interesting to integrate a position sensor in the chamber to implement a closed-loop control of its elongation. This would help to finely control the motion in the continuous mode and also facilitate the synchronization of the chambers in the step-by-step mode, especially in presence of longitudinal force. Second, the sequence was built based on temporal considerations of the component behaviors. It would be beneficial to develop a multivariable model of the actuator that would allow a control law to be implemented to improve feasible speeds. This is however challenging, as the dynamic control of the chambers has to be combined with their discrete activations.

REFERENCES

[1] R. Monfaredi, K. Cleary, and K. Sharma, "MRI Robots for Needle-Based Interventions: Systems and Technology," *Annals of biomedical engineering*, vol. 46, pp. 1479–1497, Oct. 2018.

[2] D. B. Comber, J. E. Slightam, V. R. Gervasi, J. S. Neimat, and E. J. Barth, "Design, Additive Manufacture, and Control of a Pneumatic MR-Compatible Needle Driver," *IEEE Transactions on Robotics*, vol. 32, pp. 138–149, Feb. 2016.

[3] A. Gunderman, R. Montayre, A. Ranjan, and Y. Chen, "Review of Robot-Assisted HIFU Therapy," *Sensors*, vol. 23, p. 3707, Jan. 2023.

[4] P. Cabras, P. Auloge, F. Bing, P. P. Rao, S. Hoarau, E. Dumont, A. Durand, B. Maurin, B. Wach, L. Cuvillon, E. Breton, A. Gangi, and J. Vappou, "A new versatile MR-guided high-intensity focused ultrasound (HIFU) device for the treatment of musculoskeletal tumors," *Scientific Reports*, vol. 12, p. 9095, May 2022.

[5] J. Dai, Z. He, G. Fang, X. Wang, Y. Li, C.-L. Cheung, L. Liang, I. Iordachita, H.-C. Chang, and K.-W. Kwok, "A Robotic Platform to Navigate MRI-guided Focused Ultrasound System," *IEEE Robotics and Automation Letters*, vol. 6, pp. 5137–5144, July 2021.

[6] K. Chinzei, R. Kikinis, and F. A. Jolesz, "MR Compatibility of Mechatronic Devices: Design Criteria," in *Medical Image Computing and Computer-Assisted Intervention – MICCAI'99* (C. Taylor and A. Colchester, eds.), Lecture Notes in Computer Science, (Berlin, Heidelberg), pp. 1020–1030, Springer, 1999.

[7] A. Antoniou, M. Giannakou, N. Evripidou, S. Stratis, S. Pichardo, and C. Damianou, "Robotic system for top to bottom MRgFUS therapy of multiple cancer types," *The International Journal of Medical Robotics and Computer Assisted Surgery*, vol. 18, p. e2364, Apr. 2022.

[8] W. Meinhold, D. E. Martinez, J. Oshinski, A.-P. Hu, and J. Ueda, "A Direct Drive Parallel Plane Piezoelectric Needle Positioning Robot for MRI Guided Intraspinal Injection," *IEEE Transactions on Biomedical Engineering*, vol. 68, pp. 807–814, Mar. 2021. Conference Name: IEEE Transactions on Biomedical Engineering.

[9] Z. He, Z. Dong, G. Fang, J. D.-L. Ho, C.-L. Cheung, H.-C. Chang, C. C.-N. Chong, J. Y.-K. Chan, D. T. M. Chan, and K.-W. Kwok, "Design of a Percutaneous MRI-Guided Needle Robot With Soft Fluid-Driven Actuator," *IEEE Robotics and Automation Letters*, vol. 5, pp. 2100–2107, Apr. 2020.

[10] A. Pfeil, L. Barbé, B. Wach, A. Bruyas, F. Geiskopf, M. Nierenberger, and P. Renaud, "A 3D-Printed Needle Driver Based on Auxetic Structure and Inchworm Kinematics," in *2018 ASME International Design Engineering Technical Conference*, American Society of Mechanical Engineers Digital Collection, Nov. 2018.

[11] R. Gassert, A. Yamamoto, D. Chapuis, L. Dovat, H. Bleuler, and E. Burdet, "Actuation methods for applications in MR environments," *Concepts in Magnetic Resonance Part B: Magnetic Resonance Engineering*, vol. 29B, no. 4, pp. 191–209, 2006.

[12] S. T. Mahon, A. Buchoux, M. E. Sayed, L. Teng, and A. A. Stokes, "Soft Robots for Extreme Environments: Removing Electronic Control," in *2019 2nd IEEE International Conference on Soft Robotics (RoboSoft)*, (Seoul, Korea (South)), pp. 782–787, IEEE, Apr. 2019.

[13] D. Stoianovici, A. Patriciu, D. Petrisor, D. Mazilu, and L. Kavoussi, "A New Type of Motor: Pneumatic Step Motor," *IEEE/ASME Transactions on Mechatronics*, vol. 12, pp. 98–106, Feb. 2007.

[14] Y. Chen, C. D. Mershon, and Z. T. H. Tse, "A 10-mm MR-Conditional Unidirectional Pneumatic Stepper Motor," *IEEE/ASME Transactions on Mechatronics*, vol. 20, pp. 782–788, Apr. 2015.

[15] V. Groenhuis, F. J. Siepel, and S. Stramigioli, "Miniaturization of MR Safe Pneumatic Rotational Stepper Motors," in *2019 IEEE/RSJ International Conference on Intelligent Robots and Systems (IROS)*, pp. 7150–7156, Nov. 2019.

[16] H. Sajima, H. Kamiuchi, K. Kuwana, T. Dohi, and K. Masamune, "MR-Safe Pneumatic Rotation Stepping Actuator," *Journal of Robotics and Mechatronics*, vol. 24, pp. 820–827, Oct. 2012.

[17] D. Stoianovici, D. Song, D. Petrisor, D. Ursu, D. Mazilu, M. Mutener, M. Schar, and A. Patriciu, ""MRI Stealth" robot for prostate interventions," *Minimally invasive therapy & allied technologies : MITAT : official journal of the Society for Minimally Invasive Therapy*, vol. 16, no. 4, pp. 241–248, 2007.

[18] E. Mendoza and J. P. Whitney, "A Testbed for Haptic and Magnetic Resonance Imaging-Guided Percutaneous Needle Biopsy," *IEEE Robotics and Automation Letters*, vol. 4, pp. 3177–3183, Oct. 2019.

[19] Z. Dong, Z. Guo, K.-H. Lee, G. Fang, W. L. Tang, H.-C. Chang, D. T. M. Chan, and K.-W. Kwok, "High-Performance Continuous Hydraulic Motor for MR Safe Robotic Teleoperation," *IEEE Robotics and Automation Letters*, vol. 4, pp. 1964–1971, Apr. 2019.

[20] B. Yang, U.-X. Tan, A. B. McMillan, R. Gullapalli, and J. P. Desai, "Design and Control of a 1-DOF MRI-Compatible Pneumatically Actuated Robot With Long Transmission Lines," *IEEE/ASME Transactions on Mechatronics*, vol. 16, pp. 1040–1048, Dec. 2011.

[21] V. Groenhuis and S. Stramigioli, "Laser-Cutting Pneumatics," *IEEE/ASME Transactions on Mechatronics*, vol. 21, pp. 1604–1611, June 2016.

[22] F. Schmitt, O. Piccin, B. Bayle, P. Renaud, and L. Barbé, "Inverted Honeycomb Cell as a Reinforcement Structure for Building Soft Pneumatic Linear Actuators," *Journal of Mechanisms and Robotics*, vol. 13, p. 011020, Feb. 2021.